Hole Doping in Al–Containing Nickel Oxide Materials To Improve Electrochromic Performance

8 AUTHORS, INCLUDING:

Feng Lin
Lawrence Berkeley National Laboratory
40 PUBLICATIONS   321 CITATIONS

SEE PROFILE

Dennis Nordlund
Stanford University
188 PUBLICATIONS   4,627 CITATIONS

SEE PROFILE

Ryan M Richards
Colorado School of Mines; National Renewa…
133 PUBLICATIONS   2,549 CITATIONS

SEE PROFILE

Chaiwat Engtrakul
National Renewable Energy Laboratory
64 PUBLICATIONS   1,205 CITATIONS

SEE PROFILE

Hole Doping in Al-Containing Nickel Oxide Materials To Improve Electrochromic Performance

Feng Lin,[†,‡] Dennis Nordlund,[§] Tsu-Chien Weng,[§] Rob G. Moore,[§] Dane T. Gillaspie,[†] Anne C. Dillon,[†] Ryan M. Richards,*[,‡] and Chaiwat Engtrakul*[,†]

[†]National Renewable Energy Laboratory, Golden, Colorado 80401, United States

[‡]Department of Chemistry and Geochemistry, Materials Science Program, Colorado School of Mines, Golden, Colorado 80401, United States

[§]Stanford Synchrotron Radiation Lightsource at SLAC, Menlo Park, California 94025, United States

ABSTRACT: Electrochromic materials exhibit switchable optical properties that can find applications in various fields, including smart windows, nonemissive displays, and semiconductors. High-performing nickel oxide electrochromic materials have been realized by controlling the material composition and tuning the nanostructural morphology. Post-treatment techniques could represent efficient and cost-effective approaches for performance enhancement. Herein, we report on a post-processing ozone technique that improves the electrochromic performance of an aluminum-containing nickel oxide material in lithium-ion electrolytes. The resulting materials were studied using X-ray diffraction (XRD), scanning electron microscopy (SEM), X-ray photoelectron spectroscopy (XPS), ultraviolet–visible–near-infrared (UV-vis-NIR) spectroscopy, and X-ray absorption spectroscopy (XAS). It was observed that ozone exposure increased the Ni oxidation state by introducing hole states in the NiO_6 octahedral unit. In addition, ozone exposure gives rise to higher-performing aluminum-containing nickel oxide films, relative to nickel oxide containing both Al and Li, in terms of switching kinetics, bleached-state transparency, and optical modulation. The improved performance is attributed to the decreased crystallinity and increased nickel oxidation state in aluminum-containing nickel oxide electrochromic films. The present study provides an alternative route to improve electrochromic performance for nickel oxide materials.

KEYWORDS: lithium, nickel oxide, ozone, electrochromic, oxidation state, aluminum
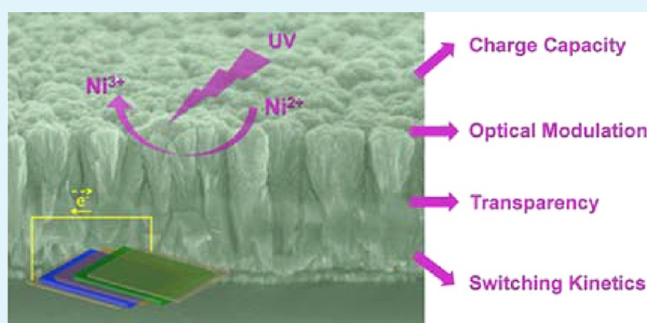
■ INTRODUCTION

Since the initial reports by Deb in 1969[1] and 1973,[2] inorganic electrochromic materials have been investigated intensively for smart windows, automobile rear-view mirrors, and nonemissive display applications. Electrochromic materials perform via the reversible modulation of optical characteristics upon charge/discharge of ions (e.g., Li^+, H^+) and charge-compensating electrons. Thus far, many transition-metal oxides (e.g., nickel oxide, tungsten oxide, titanium oxide) have been reported to possess electrochromic properties,[3−5] as well as some organic materials (e.g., conjugated polymers).[6] Inorganic electrochromic materials have received tremendous attention, because of their stability against sunlight exposure and ease of fabrication using conventional sputtering techniques. A typical inorganic electrochromic device configuration is shown in Scheme 1, where tungsten oxide and nickel oxide are the cathodic and anodic electrodes, respectively.[7,8] This configuration affords a more neutral color in the dark state and enhances occupant comfort (aesthetic appeal) and productivity in buildings.[8] In addition, the electrochromic coloration efficiency is increased for this device configuration, because of the dual contributions from two active electrodes.[9]

The practical operation of inorganic electrochromic devices is reliant on the development of tungsten oxide and nickel oxide electrochromic materials. To date, significant efforts have been successfully dedicated to achieve high-performing tungsten oxide cathodic materials via various deposition techniques.[3,10−12] In contrast, nickel oxide anodic materials still tend to suffer from relatively poor performance (i.e., inferior optical modulation, slow switching kinetics, poor bleached-state transparency), thus limiting large-area window applications.[8,13−16] Specifically, residual absorption between 400 and 500 nm in the bleached state leads to an aesthetically unpleasant yellowish color and reduces the collection of sunlight.[17] Avendano et al. reported improved transparency in the visible wavelength range in nickel oxide films containing Mg, Al, Si, Zr, Nb, or Ta in aqueous alkaline electrolytes.[17]
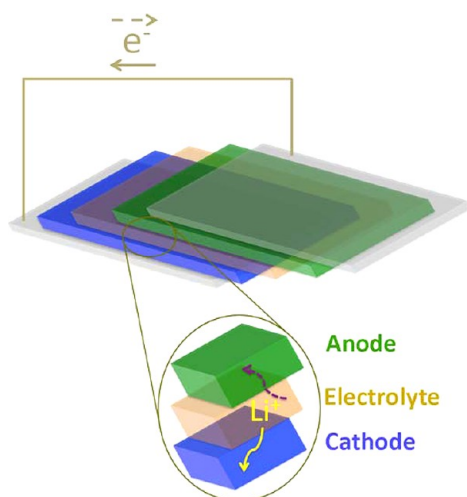
e^-

Anode
Electrolyte
Li
Cathode

[a]The solid (yellow) and dashed (purple) arrows represent the
coloration and bleaching processes, respectively.

Optical spectroscopy studies suggested that these additives
were indeed dopants in the conventional sense with the ability
to form oxides with large optical band gaps.[8,17] Furthermore, in
a recent report by Gillaspie et al., a thin film nickel oxide-based
electrode with multiple additives was prepared from a
composite ceramic sputter target produced from Li_2CO_3,
NiO, and WO_3 powders.[9] Here, the authors demonstrated
that the bleached state of the $Li_{1.2}NiW_{0.1}O_x$ nanocomposite
counter electrode was ca. 35% higher than that of a similarly
prepared $LiNiO_x$ film at 670 nm. Even though high-performing
nickel oxide materials have been obtained by controlling
material composition[9,18] or tuning nanostructural morphol-
ogy,[19,20] these processes typically involve time-consuming
procedures (e.g., ceramic target preparation)[9,18] and wet-
chemical solution processing steps.[21] Alternatively, efficient
post-processing techniques could facilitate improvements in
material properties and provide a general route for enhancing
electrochromic performance.

Post-processing treatments are typically performed at low
temperatures in order to inhibit the crystallization (particle
growth) of electrochromic materials. Electrochromic materials
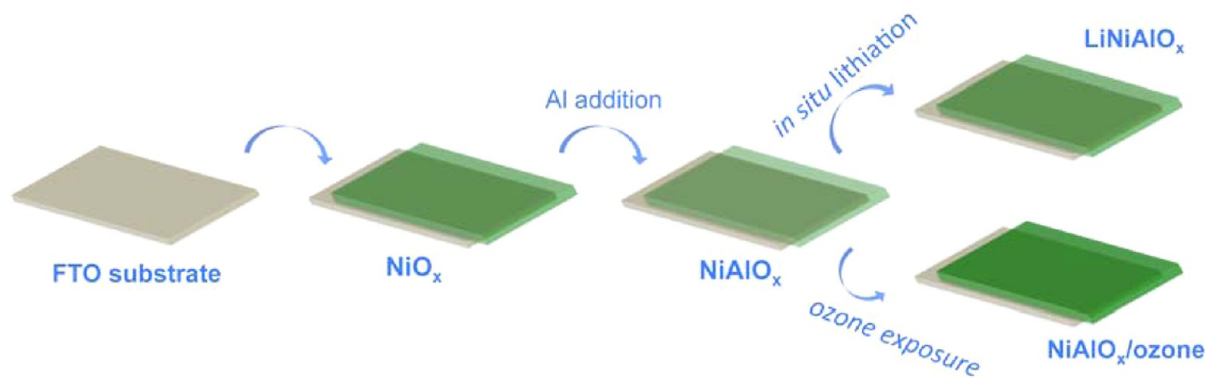that possess low crystallinity (small particle size) tend to have

fast charge/discharge rates (i.e., fast switching kinetics or
response times), potentially offering faster switching electro-
chromic coatings.[22,23] A low-temperature ozone exposure
technique was previously employed to modify the stoichiom-
etry and surface crystallinity and enhance the electrochromic
performance for tungsten oxide materials.[12] Moreover, the
treatment of as-deposited nickel oxide films with ozone was
found to alter the surface species (chemistry), resulting in
higher oxidation states of nickel.[24,25] It is anticipated that the
electrochromic properties of nickel oxide-based films will be
strongly correlated with the surface states, as dictated by post-
processing treatments. Alternatively, lithium doping (incorpo-
ration of hole states) has also been shown to increase the
oxidation state of nickel in nickel oxide.[26,27] Here, the hole
states in the Li-doped nickel oxide material were associated
with the NiO_6 octahedral unit.[26] Electrochromism in nickel
oxide is expected to arise from the reversible Ni^{2+}/Ni^{3+} redox
couple.[8] Therefore, the incorporation of hole states in as-
deposited nickel oxide materials are expected to play a
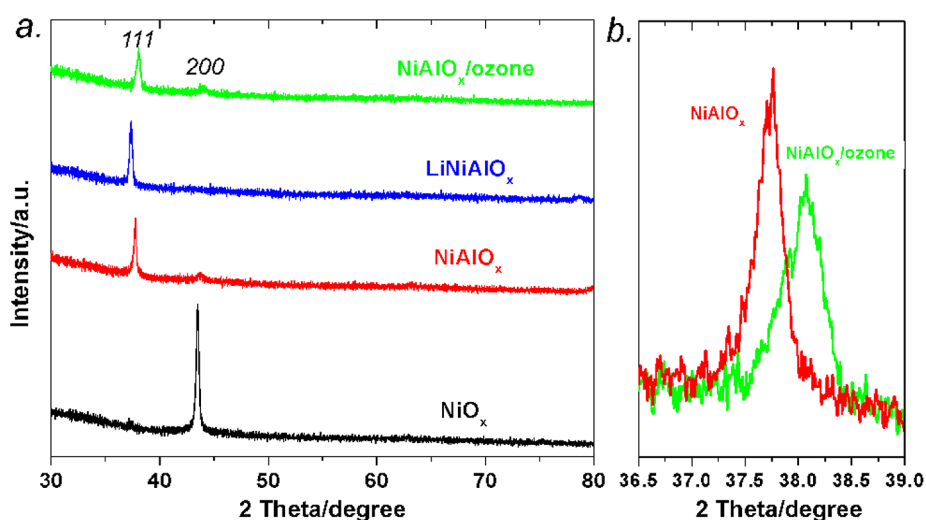significant role in the electrochromic process.

Herein, we report on post-processing treatments that
introduce hole states and enhance the electrochromic proper-
ties in nickel oxide materials. Ozone exposure and in situ
lithiation (i.e., lithium doping) are shown to increase hole states
and significantly improve optical modulation for Al-containing
nickel oxide electrochromic films. Comprehensive electro-
chromic evaluation demonstrates that ozone exposure is
superior to in situ lithiation, in terms of maintaining fast
switching kinetics, high bleached-state transparency, and large
optical modulation, because of the decreased crystallinity and
increased nickel oxidation state.

■ EXPERIMENTAL METHODS

Fabrication of Electrochromic Films. The sample preparation is
schematically presented in Scheme 2. Radio-frequency magnetron
sputtering (Angstrom EvoVac deposition system housed in a glovebox
under an argon atmosphere) was employed to deposit electrochromic
films ∼300 nm thick, using either a Ni metal target, Ni−Al alloy target
(Ni/Al 90/10 at%), or Ni−Al alloy target (Ni/Al 90/10 at%) and Li_2O
ceramic target for nickel oxide, Al-containing nickel oxide, and Li-
doped Al-containing nickel oxide, respectively. The Ni metal and Ni−
Al alloy targets were purchased from ACI Alloys, while the Li_2O
ceramic target supported on a molybdenum backing plate was
purchased from Plasmaterials, Inc. The gun powers for metallic targets
(e.g., Ni, Ni/Al) and ceramic target (i.e., Li_2O) were 120 and 45 W,
respectively. It is noted that the Li_2O co-sputtering process is hereafter
denoted as in situ lithiation. The electrochromic films were deposited
onto either F-doped SnO_2 (F: SnO_2) coated glass (TEC 15, Hartford

Scheme 2. Schematic Illustration of the Preparation for Electrochromic Films

FTO substrate　　NiO$_x$　　Al addition　　NiAlO$_x$　　in situ lithiation　　LiNiAlO$_x$

ozone exposure　　NiAlO$_x$/ozone

　　　　dx.doi.org/10.1021/am302097b | *ACS Appl. Mater. Interfaces* 2013, 5, 301−309

Figure 1. (a) XRD patterns for the as-deposited electrochromic films and (b) the magnification for the NiO (111) peaks of NiAlO$_x$ and NiAlO$_x$/ozone electrochromic films.
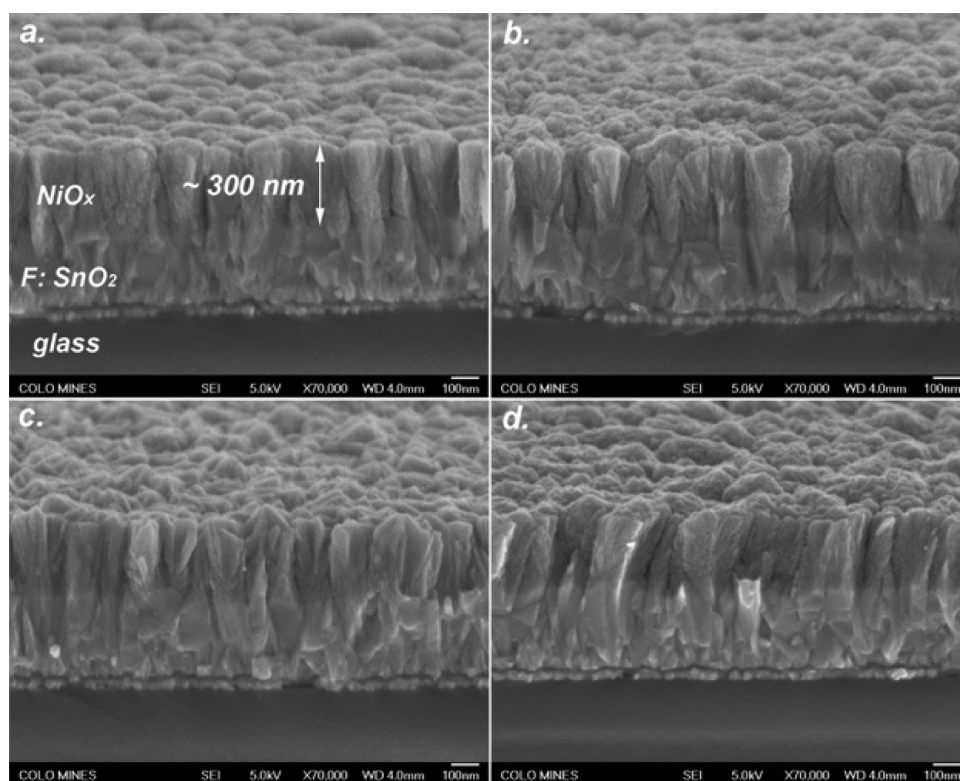
Figure 2. Cross-sectional SEM images for the as-deposited electrochromic films: (a) NiO$_x$, (b) NiAlO$_x$, (c) LiNiAlO$_x$, and (d) NiAlO$_x$/ozone, where the samples were tilted 15°. The layer identification is exemplified in panel a.

Glass Co., Inc.) or regular microscope glass (VWR Scientific). The substrates were cleaned successively with soapy water, acetone, isopropanol, and deionized (DI) water, and subsequently dried under a N$_2$ gun. The target–substrate distance was held constant at 10 cm and no additional heating was applied to the substrate. The base pressure and total deposition pressure were 10^{-7} Torr and 3 mTorr, respectively. The Ar/O$_2$ ratio was fixed at 4/1 throughout the study. Low-temperature ozone exposure was described elsewhere.[12] Briefly, the process was performed in a UV surface decontamination system equipped with a heat controller (Novascan Technologies, Inc.). The sample chamber was purged with pure oxygen for 1 min prior to initiating heating and UV irradiation. The samples were exposed to ozone for 30 min at 100 °C. For simplicity, the Al-containing nickel

oxide, Li-doped Al-containing nickel oxide, and ozone-exposed Al-containing oxide are hereafter denoted as NiAlO$_x$, LiNiAlO$_x$, and NiAlO$_x$/ozone, respectively.

Characterization of Electrochromic Films. The crystal structures of the resulting films were characterized on a Philips X-ray diffractometer (Model PW1729) operated at 45 kV and 40 mA, using Cu Kα radiation. Transmittance and reflectance measurements were performed on a Cary 6000i UV-vis-NIR spectrometer. Scanning electron microscopy (SEM) was done on a JEOL Model JSM-7000F field-emission scanning electron microscope with an EDAX Genesis EDS. X-ray photoelectron spectroscopy (XPS) was performed on a Kratos Axis HSi Ultra X-ray photoelectron spectrometer, using an Al Kα X-ray source operated at 14 kV and 10 mA. X-ray absorption

spectroscopy (XAS) measurements were performed on the 31-pole wiggler beamline 10-1 at the Stanford Synchrotron Radiation Lightsource (SSRL), using a ring current of 350 mA and a 1000 mm^{-1} spherical grating monochromator, with a 20-μm entrance and exit slits providing an energy resolution of 0.1 eV. All data were acquired in a single load at room temperature and under ultrahigh vacuum (10^{-9} Torr) in total electron yield (TEY) mode and fluorescence yield (FY) mode. For TEY, we collected the sample drain current, and a silicon diode (IRD AXUV-100) was used to collect the FY positioned near the sample surface. Contributions from visible light were carefully minimized before the acquisition, and all spectra were normalized by the current from freshly evaporated gold on a fine grid positioned upstream of the main chamber. Samples were mounted on an aluminum holder attached to the main chamber manipulator.

Electrochromic Evaluation. Electrochromic performance was evaluated in a liquid electrolyte half-cell where the electrolyte was 1 M lithium perchlorate ($LiClO_4$) dissolved in propylene carbonate (i.e., $LiClO_4$−PC). Cyclic voltammetry (CV) was carried out using a BioLogic VMP3 multichannel potentiostat with a scan rate of 20 mV/s and a voltage range of 1.7−4.2 V vs Li/Li$^+$. In situ transmittance was measured using a diode laser at 670 nm with a blank F:SnO$_2$ coated glass for background correction (i.e., 100% transmittance). Switching kinetics (i.e., coloration, bleaching) were evaluated under chronoamperometry (CA) cycling from 1.7 V to 4.2 V vs Li/Li$^+$, where each potential step was maintained for 2 min to ensure the saturation of current (i.e., Li$^+$/electron saturation). The switching kinetics measurement was continued for 300 cycles. The switching speed is defined as the time required to achieve ~90% of total transmittance change within a potential step. The samples were transferred between the sputtering chamber and testing cells without exposure to air or moisture. All electrochemical measurements were carried out under an argon atmosphere in a glovebox.

■ RESULTS AND DISCUSSION

Figure 1 presents the XRD patterns for the as-deposited electrochromic films. The patterns are consistent with the standard face-centered cubic NiO (Joint Committee for Powder Diffraction Standards (JCPDS) File Card No. 65-2901, $Fm\overline{3}m$ (225)).[28] The NiO$_x$ electrochromic film shows distinct crystal orientation relative to the other electrochromic films (NiAlO$_x$, LiNiAlO$_x$, and NiAlO$_x$/ozone). The NiO (100) plane of NiO$_x$ is oriented horizontally, with respect to the substrate surface, while NiAlO$_x$, LiNiAlO$_x$, and NiAlO$_x$/ozone films are horizontally oriented along the NiO (111) plane. It is likely that the addition of Al affected the growth orientation of nickel oxide. No major difference was observed for the LiNiAlO$_x$ and NiAlO$_x$ electrochromic films, indicating that Li does not further alter the growth behavior of the NiAlO$_x$ electrochromic film. Importantly, the NiAlO$_x$ electrochromic film is amorphized (i.e., crystallinity decreases) after ozone exposure, as indicated by the increase of full width at half-maximum (fwhm) of the NiO(111) peak (Figure 1b). This is consistent with our previous finding, where a low-temperature ozone exposure technique was used to optimize the electrochromic performance of WO$_x$ nanorod materials.[12] Furthermore, the lattice size of NiAlO$_x$/ozone electrochromic film is decreased, relative to that of the NiAlO$_x$ electrochromic film indicated by the shift of diffraction angle (Figure 1b). The exact mechanism for the change in lattice size is unclear at this point.

The morphologies of the as-deposited electrochromic films are shown in Figure 2. A strong adhesion is observed between film and substrate for all samples, which is critical for electron transport from the external circuit to electrochromic films (as shown in Scheme 1) and mechanical stability.[18] The electrochromic films show a uniform thickness of ~300 nm. This
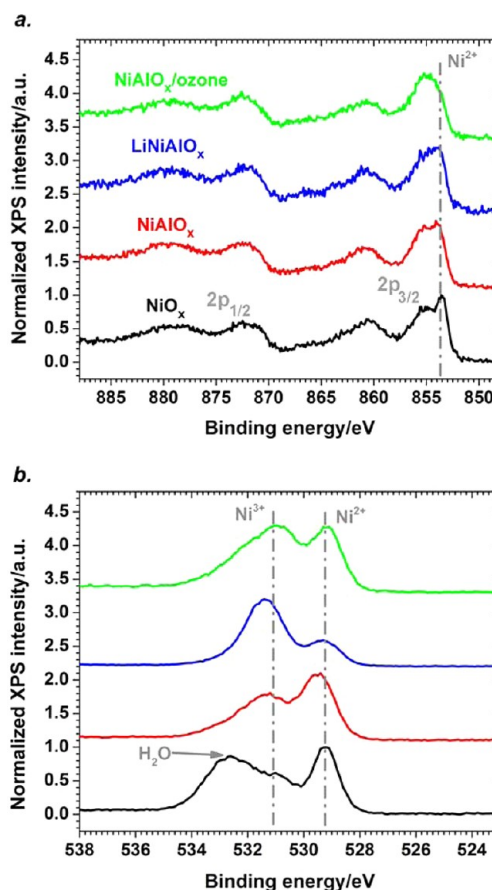

Figure 3. XPS spectra of the NiO$_x$ (black), NiAlO$_x$ (red), LiNiAlO$_x$ (blue), and NiAlO$_x$/ozone (green) electrochromic films: (a) Ni 2p and (b) O 1s.
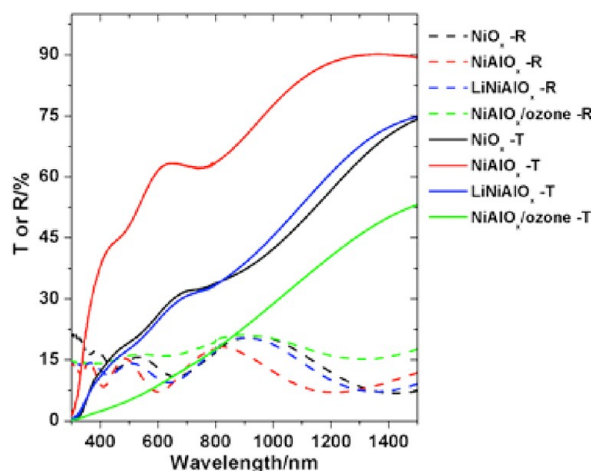
Figure 4. Transmittance and reflectance spectra for the as-deposited electrochromic films, and the solid and dashed spectra represent the transmittance (T) and reflectance (R), respectively. The black, red, blue, and green spectra represent NiO$_x$, NiAlO$_x$, LiNiAlO$_x$, and NiAlO$_x$/ozone electrochromic films, respectively.

uniform film thickness is crucial for conducting a direct comparison between different films since electrochromic performance metrics are typically dependent on film thickness.[29] The degree of surface roughness (surface area) increases after Al addition (Figure 2a vs Figure 2b), thus enhancing electrolyte−electrode interactions and possibly leading to faster
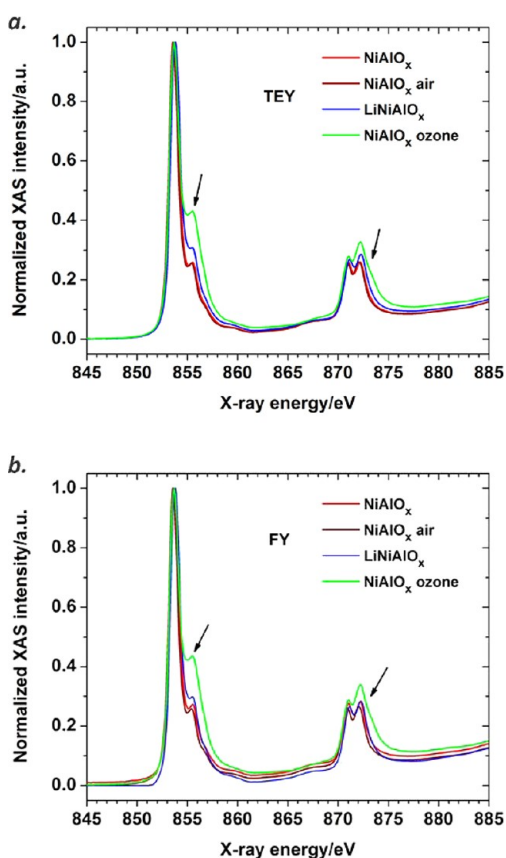
Figure 5. Ni L-edge X-ray absorption spectra for the Al-containing nickel oxide electrochromic films: (a) total electron yield (TEY) mode and (b) fluorescence yield (FY) mode. The red, purple, blue, and green spectra represent NiAlO$_x$, air-exposed NiAlO$_x$, LiNiAlO$_x$, and NiAlO$_x$/ozone, respectively.

charge/discharge rates in the electrochromic film. The cross-sectional particle agglomeration converts from a column-like to blade-like morphology for the electrochromic film prepared with in situ lithiation (see Figure 2b vs Figure 2c). Interestingly, the morphology of the NiAlO$_x$ film remains unaltered after ozone exposure, compared to the NiAlO$_x$ film (see Figure 2b vs Figure 2d), unlike for UV processed TiO$_2$[30] and SnO$_2$[31] thin films.

High-resolution XPS spectra are sensitive to the chemical oxidation states present on the surface of a thin film. XPS Ni 2p and O 1s spectra have been previously used to determine nickel oxidation states of complex surface species in nickel oxide-based materials.[32−34] Several studies have shown that the relative concentration of Ni^{2+} and Ni^{3+} could be modified with compositional engineering[26] and post-processing treatments.[24] These studies shed light on the interpretation of the present XPS data. The Ni 2p and O 1s spectra are shown in Figures 3a and 3b, respectively. The 2p photoelectron spectra of first-row transition metals typically show additional energy loss features in addition to the 2p spin-orbit doublets.[35] The Ni 2p$_{3/2}$ spectrum of NiO$_x$ displays a lower binding energy feature at 853.7 eV, which is attributed to the Ni^{2+} species (e.g., NiO) in the NiO$_x$ electrochromic film.[36] This is consistent with our XRD result (Figure 1) that NiO is the dominant phase in the nickel oxide-based films. In situ lithiation and ozone exposure decrease the relative intensity of this lower binding energy peak (853.7 eV), as opposed to higher binding energy peaks (855.4 eV) originating from the Ni^{3+} oxidation state.[34,35] The XPS O

1s spectrum also provides useful information pertaining to the oxidation state of nickel.[32] The peak ascribed to O 1s of NiO is observed for all electrochromic films between 529.1 eV and 529.3 eV. In addition, a higher binding energy peak is observed between 531.1 eV and 531.4 eV, which is attributed to the O 1s of trivalent nickel oxide (e.g., Ni$_2$O$_3$, NiOOH).[32,34] The increase in intensity of the O 1s signals at 531.4 eV for LiNiAlO$_x$ and 531.0 eV for NiAlO$_x$/ozone suggest that there is an increase in the concentration of Ni^{3+} species in these samples. The peak at the higher binding energy (532.6 eV) is attributed to physisorbed H$_2$O in the NiO$_x$ film.[24] The physisorbed H$_2$O is significantly decreased for the electrochromic films containing additional additives (NiAlO$_x$, LiNiAlO$_x$, and NiAlO$_x$/ozone) relative to the pristine NiO$_x$. Based on the discussion above, we tentatively conclude that in situ lithiation and ozone exposure increase the concentration of Ni^{3+} species in the Al-containing nickel oxide electrochromic materials. Since XPS is a surface-sensitive technique, features in the O 1s spectra can be related to the adsorption (formation) of oxygen-containing surface species (e.g., CO$_3^{2-}$) and cannot be ruled out. In addition, we note that the interpretation of the Ni 2p and O 1s spectra for nickel oxide has remained a topic of intense study.[37,38] Therefore, to substantiate our claim that in situ lithiation and ozone exposure increase the concentration of Ni^{3+} species in the Al-containing nickel oxide electrochromic materials, additional characterization techniques including UV-vis-NIR transmittance spectroscopy and XAS were employed and discussed below.

UV-vis-NIR transmittance spectroscopy is an informative technique to study the bulk chemical properties of nickel oxide and has the ability to differentiate between Ni^{2+} and Ni^{3+} species in nickel oxide films.[25,39,40] Aluminum is known to act as an electron donor and fill the hole states in NiO$_x$; therefore, a low absorption in NiAlO$_x$ is expected.[17] As shown in Figure 4, the addition of Al in NiO$_x$ leads to a significant increase in transmittance. The in situ lithiation of NiAlO$_x$ results in decreased transmittance, since Li acts as a p-type dopant (i.e., increases Ni oxidation states) for nickel oxide material.[41] Ozone exposure also decreases the transmittance of the NiAlO$_x$ electrochromic film, because of the increase in Ni^{3+} concentration.[24] Therefore, both ozone exposure and in situ lithiation increase the concentration of hole states (i.e., increase in Ni^{3+} concentration) in NiAlO$_x$ films, but it should be noted that the LiNiAlO$_x$ films exhibit a lower hole concentration than the NiAlO$_x$/ozone films. Our present study confirms previous experimental and theoretical studies on the nature of the hole states in nickel oxide, where holes are associated with (localized on) the octahedral NiO$_6$ unit.[26,27] Finally, it is noted that the reflectance properties of the nickel oxide-based films are slightly altered, depending on material composition (dashed curves in Figure 4).

To probe the nickel oxidation states and hole doping in the nickel oxide-based electrochromic films in more detail, XAS was performed for Ni L-edge in both total electron yield (TEY) (surface-sensitive) and fluorescence yield (FY) (bulk-sensitive) modes to validate the analysis above. The Ni L-edge corresponds to the dipole allowed transitions from Ni 2p to Ni 3d states, including Ni 2p$_{3/2}$ and Ni 2p$_{1/2}$ spin-orbit final states. It is noted that the Ni L-edge XAS spectra for the as-deposited electrochromic films are consistent with previously reported spectra (see Figure 5).[26,42] The spectra clearly exhibit the characteristic features for spin-orbit effects, Ni 2p−Ni 3d electrostatic interactions, and crystal field effects. The features
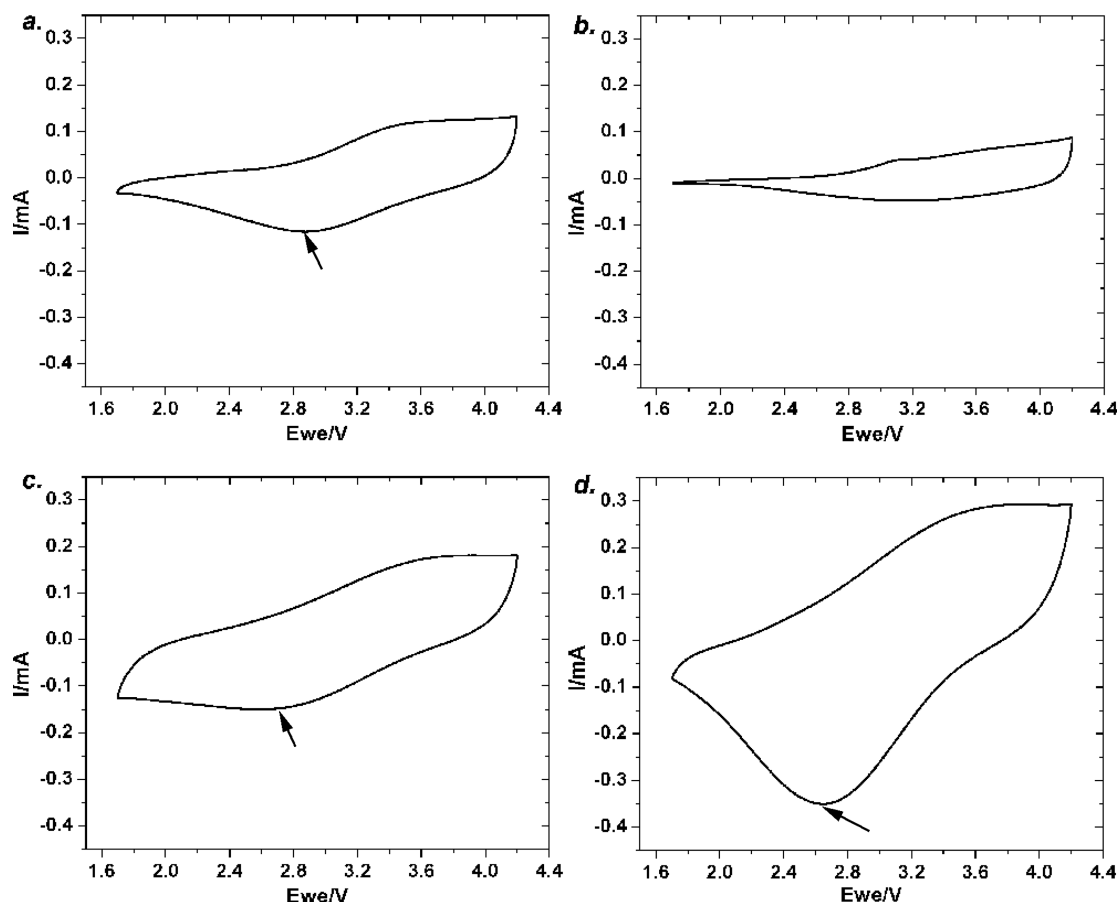
Figure 6. CV curves (100th cycle) for (a) NiO_x, (b) $NiAlO_x$, (c) $LiNiAlO_x$, and (d) $NiAlO_x$/ozone, where the arrows indicate the cathodic peaks.
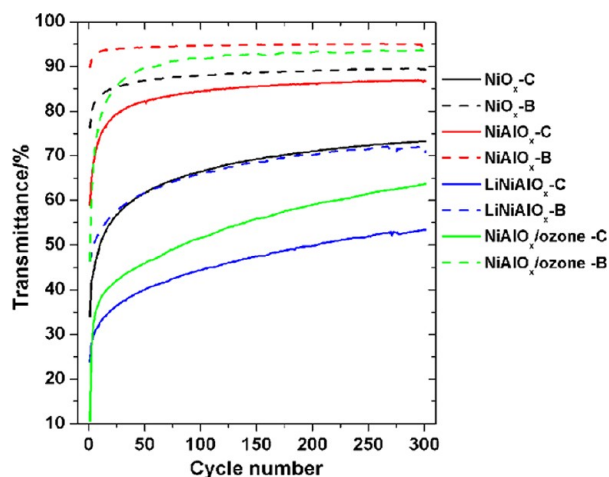

Figure 7. Dependence of in situ transmittance on CV cycle number, where B (the dashed curve) and C (the solid curve) represent bleached and colored states, respectively; the difference between these two transmittance values is interpreted as the optical modulation. The in situ transmittance is taken at 670 nm.

Figure 8. Absorbance spectra for the electrochromic films after the discharge process (i.e., Li^+/e^- intercalation).

in Figure 5 denoted by the arrows are sensitive to the formal Ni oxidation state. Generally, an increase in the intensities of these features indicates an increase in the hole concentration on the NiO_6 octahedral unit (i.e., increase in Ni^{3+} concentration).[26,42] The Ni L-edge XAS results are in agreement with the corresponding XPS and UV-vis-NIR spectroscopy results, namely, that in situ lithiation and ozone exposure increase
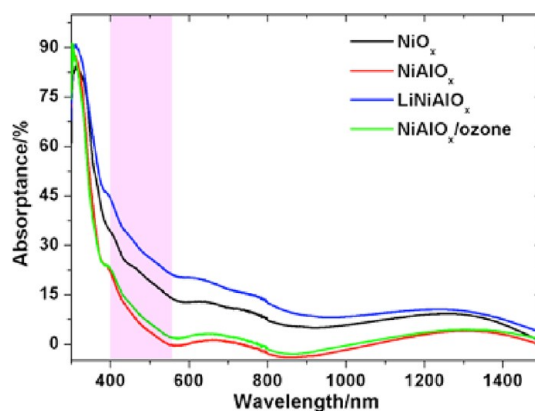
the concentration of Ni^{3+} species in the Al-containing nickel oxide materials. In addition, XAS indicates that ozone exposure is more efficient at increasing the concentration of hole states in $NiAlO_x$, in agreement with the UV-vis-NIR spectroscopy data (Figure 4). It is important to note that air exposure does not affect the nickel oxidation states in $NiAlO_x$ (Figure 5). Finally, the similarities in the Ni L-edge XAS performed in both TEY (surface-sensitive) and FY (bulk-sensitive) modes for the various Al-containing nickel oxide materials suggest that ozone exposure is capable of modifying the hole concentration throughout the entire electrochromic film. We attribute the

306

dx.doi.org/10.1021/am302097b | ACS Appl. Mater. Interfaces 2013, 5, 301–309
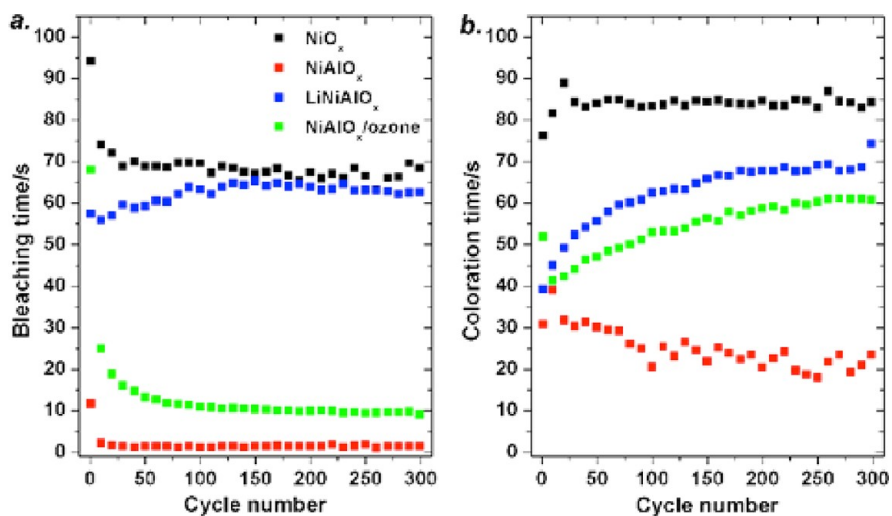
Figure 9. Dependence of (a) bleaching kinetics and (b) coloration kinetics of electrochromic films on the number of potential step cycles. The black, red, blue, and green data represent information regarding NiO_x, $NiAlO_x$, $LiNiAlO_x$ and $NiAlO_x$/ozone electrochromic films, respectively.

efficient diffusion of ozone throughout the film to the morphology observed in Figure 2.

Cyclic voltammetry (CV) and in situ transmittance measurements were used to investigate the redox and coloration/bleaching properties of the nickel oxide films. Figure 6 shows the CV curves (100th cycle) for the as-deposited electrochromic films. The addition of Al leads to significant decreases in the cathodic and anodic peak currents (see Figure 6a vs Figure 6b), indicating that the diffusion of Li$^+$ is compromised under the CV cycling conditions.[43] In contrast, in situ lithiation and ozone exposure increase the peak currents, resulting in much higher charge/discharge capacities (see Figures 6c and 6d). The increase in peak current is beneficial for decreasing operating potentials and reducing electrical energy consumption and potentially imparting durability to the device.[43] The intercalation (cathodic) peak voltages for the $LiNiAlO_x$ and $NiAlO_x$/ozone electrochromic films are indeed shifted to lower voltages, relative to the cathodic peak for the NiO_x electrochromic film.

The in situ transmittance values for the bleached and dark states are shown in Figure 7, as a function of cycle number. A significant increase in transmittance for both bleached and dark states is observed for all samples during the thin film activation period (initial 25 cycles).[18] The addition of Al into NiO_x allows the film to cycle at an elevated transmittance range; however, the optical modulation of the resulting film is compromised. This observation indicates that the addition of Al to nickel oxide is suitable for lowering bleached-state absorption in nickel oxide-based electrochromic materials functioning in lithium-ion electrolytes. Nevertheless, the optical modulation of $NiAlO_x$ is not practical for device operation. In situ lithiation increases optical modulation but decreases the bleached-state transparency in $LiNiAlO_x$. It should be noted that a further increase in lithium concentration leads to a further decrease in the bleached-state transparency for the $LiNiAlO_x$ film (data not shown). Conversely, the $NiAlO_x$/ozone film exhibits the largest optical modulation, in addition to a superior bleached-state transparency. Based on our previous discussion, we suggest that ozone exposure is superior to in situ lithiation, because of the amorphization of the surface species on the nickel oxide crystallites. Note that the stability of the optical modulation in these electrochromic films has not been optimized but may be

improved through the addition of a surface barrier layer or coating (e.g., Al_2O_3[44] and $LiAlF_4$[45,46]).

In order to investigate the full-spectrum bleached-state transparency and the effectiveness of ozone exposure for removing the residual absorption in the bleached state, the electrochromic films were cycled with chronoamperometry (CA) at 1.7 V vs Li$^+$/Li for 5 min and analyzed by UV-vis-NIR spectroscopy (Figure 8). Spectral absorptance, $A(\lambda)$, was calculated from eq 1:

$$A(\lambda) = 100\% - T(\lambda) - R(\lambda) \tag{1}$$

where $T(\lambda)$ and $R(\lambda)$ are the transmittance and reflectance, respectively. The strong absorbance below 350 nm is attributed to the band-gap absorption of nickel oxide materials. A significant decrease of $A(\lambda)$ is observed with the addition of Al, especially in the 400−550 nm wavelength region (highlighted in Figure 8). This observation is similar to a study by Avendaño et al., where transition-metal additives also lowered the bleached-state absorption in nickel oxide.[17] The low absorptance is maintained for the $NiAlO_x$/ozone electrochromic film but increases for the $LiNiAlO_x$ electrochromic film. The extent of hole removal in the NiO_6 unit through interaction with intercalated electrons and Li ions determines the quality of the bleached-state transparency. Even though the $LiNiAlO_x$ electrochromic film exhibits a lower hole concentration than the $NiAlO_x$/ozone electrochromic film in the as-deposited state (Figures 4 and 5), the existing Li ions from in situ lithiation inhibit the subsequent Li$^+$ intercalation in $LiNiAlO_x$ during the electrochemical discharge process, resulting in an inferior bleached-state transparency.

Electrochromic switching kinetics is another important parameter that is used to evaluate charge transfer and Li$^+$ diffusion in electrochromic materials and must be considered during device fabrication. Here, switching kinetics (bleaching and coloration times) for the nickel oxide-based films was measured using a CA cycling technique (Figure 9). Overall, bleaching kinetics are faster than coloration kinetics for all of the studied electrochromic films after 150 CA cycles. Surprisingly, the addition of Al into NiO_x accelerates the bleaching kinetics of NiO_x by a factor of ∼70 (see Figure 9a) and the coloration kinetics increase by a factor of ∼4 (see Figure 9b). The switching kinetics was compromised after in

307

dx.doi.org/10.1021/am302097b | ACS Appl. Mater. Interfaces 2013, 5, 301−309

situ lithiation and ozone exposure were applied to $NiAlO_x$. Nevertheless, the post-processing ozone technique is more effective for maintaining fast switching kinetics than the in situ lithiation approach. We have clearly demonstrated that ozone exposure is superior to in situ lithiation for optimizing the extent and rate of hole removal in nickel oxide-based materials, subsequently enhancing bleached-state transparency and bleaching kinetics, respectively. Based on our material characterization discussion, the superior performance is most likely due to the amorphization of the nickel oxide crystallites afforded by ozone exposure. The amorphization of transition-metal-based electrochromic materials has been shown to facilitate (improve) lithium diffusion.[13,47]

CONCLUSION

Nickel oxide-based electrochromic films were prepared via magnetron sputtering. The performance of these electrochromic films was evaluated in a Li-ion electrolyte. Electron-donating elements (e.g., Al) decrease bleached-state absorption of nickel oxide electrochromic films but do not create/increase reasonable optical modulation in Li-ion electrolyte. In situ lithiation and ozone exposure increase the hole states in the $NiAlO_x$ electrochromic film and enhance optical modulation. Nickel oxide films containing Al exhibit superior electrochromic properties after ozone exposure, relative to nickel oxide films containing Al and Li (in situ lithiation). We infer that ozone exposure creates hole states (i.e., Ni^{3+} species) mainly on the surface of the nickel oxide crystallites (particles), thus shortening the diffusion length of the intercalating electrons.

AUTHOR INFORMATION

Corresponding Author

*E-mails: rrichard@mines.edu (R.M.R.), chaiwat.engtrakul@nrel.gov (C.E.).

Author Contributions

F.L., D.T.G., and C.E. conceived and designed the project and experiments. F.L. synthesized and characterized the thin films studied in this work. D.N., T.C.W., and R.G.M. performed the XAS experiments. A.C.D., R.M.R., and C.E. supervised and directed the work. F.L., R.M.R., and C.E. wrote the manuscript.

Notes

The authors declare no competing financial interest.

ACKNOWLEDGMENTS

REFERENCES

(1) Deb, S. K. *Appl. Opt. Suppl.* **1969**, 3, 192−195.
(2) Deb, S. K. *Philos. Mag.* **1973**, 27 (4), 801−822.
(3) Gil-Rostra, J.; Cano, M.; Pedrosa, J. M.; Ferrer, F. J.; Garcia-Garcia, F.; Yubero, F.; Gonzalez-Elipe, A. R. *ACS Appl. Mater. Interfaces* **2012**, 4 (2), 628−638.
(4) Xia, X. H.; Tu, J. P.; Zhang, J.; Xiang, J. Y.; Wang, X. L.; Zhao, X. B. *ACS Appl. Mater. Interfaces* **2010**, 2 (1), 186−192.
(5) Ghicov, A.; Yamamoto, M.; Schmuki, P. *Angew. Chem., Int. Ed.* **2008**, 47 (41), 7934−7937.
(6) Beaujuge, P. M.; Reynolds, J. R. *Chem. Rev.* **2010**, 110 (1), 268−320.
(7) Granqvist, C. R. *Nat. Mater.* **2006**, 5 (2), 89−90.
(8) Gillaspie, D. T.; Tenent, R. C.; Dillon, A. C. *J. Mater. Chem.* **2010**, 20 (43), 9585−9592.
(9) Gillaspie, D.; Norman, A.; Tracy, C. E.; Pitts, J. R.; Lee, S. H.; Dillon, A. *J. Electrochem. Soc.* **2010**, 157 (3), H328−H331.
(10) Brezesinski, T.; Fattakhova-Rohlfing, D.; Sallard, S.; Antonietti, M.; Smarsly, B. M. *Small* **2006**, 2 (10), 1203−1211.
(11) Lee, S. H.; Deshpande, R.; Parilla, P. A.; Jones, K. M.; To, B.; Mahan, A. H.; Dillon, A. C. *Adv. Mater.* **2006**, 18 (6), 763−766.
(12) Lin, F.; Li, C. P.; Chen, G.; Tenent, R. C.; Wolden, C. A.; Gillaspie, D. T.; Dillon, A. C.; Richards, R. M.; Engtrakul, C. *Nanotechnology* **2012**, 23 (25), 255601.
(13) Lee, S. H.; Park, Y. S.; Joo, S. K. *Solid State Ionics* **1998**, 109 (3−4), 303−310.
(14) Bouessaya, I.; Rougier, A.; Poizot, P.; Moscovici, J.; Michalowicz, A.; Tarascon, J. M. *Electrochim. Acta* **2005**, 50 (18), 3737−3745.
(15) Penin, N.; Rougier, A.; Laffont, L.; Poizot, P.; Tarascon, J. M. *Sol. Energy Mater. Sol. Cells* **2006**, 90 (4), 422−433.
(16) Smulko, J.; Azens, A.; Marsal, R.; Kish, L. B.; Green, S.; Granqvist, C. G. *Sol. Energy Mater. Sol. Cells* **2008**, 92 (8), 914−918.
(17) Avendano, E.; Azens, A.; Niklasson, G. A.; Granqvist, C. G. *Sol. Energy Mater. Sol. Cells* **2004**, 84 (1−4), 337−350.
(18) Moulki, H.; Park, D. H.; Min, B.-K.; Kwon, H.; Hwang, S.-J.; Choy, J.-H.; Toupance, T.; Campet, G.; Rougier, A. *Electrochim. Acta* **2012**, 74, 46−52.
(19) Yoshino, T.; Kobayashi, K.; Araki, S.; Nakamura, K.; Kobayashi, N. *Sol. Energy Mater Sol. Cells* **2012**, 99, 43−49.
(20) Xia, X. H.; Tu, J. P.; Zhang, J.; Wang, X. L.; Zhang, W. K.; Huang, H. *Sol. Energy Mater Sol. Cells* **2008**, 92 (6), 628−633.
(21) Yuan, Y. F.; Xia, X. H.; Wu, J. B.; Chen, Y. B.; Yang, J. L.; Guo, S. Y. *Electrochim. Acta* **2011**, 56 (3), 1208−1212.
(22) Lin, F.; Cheng, J. F.; Engtrakul, C.; Dillon, A. C.; Nordlund, D.; Moore, R. G.; Weng, T. C.; Williams, S. K. R.; Richards, R. M. *J. Mater. Chem.* **2012**, 22 (33), 16817−16823.
(23) Park, S. Y.; Lee, J. M.; Noh, C.; Son, S. U. *J. Mater. Chem.* **2009**, 19 (42), 7959−7964.
(24) Ratcliff, E. L.; Meyer, J.; Steirer, K. X.; Garcia, A.; Berry, J. J.; Ginley, D. S.; Olson, D. C.; Kahn, A.; Armstrong, N. R. *Chem. Mater.* **2011**, 23 (22), 4988−5000.
(25) Azens, A.; Kullman, L.; Granqvist, C. G. *Sol. Energy Mater. Sol. Cells* **2003**, 76 (2), 147−153.
(26) Vanveenendaal, M. A.; Sawatzky, G. A. *Phys. Rev. B* **1994**, 50 (16), 11326−11331.
(27) Chen, H. R.; Harding, J. H. *Phys. Rev. B* **2012**, 85, 11.
(28) Hu, J. C.; Zhu, K. K.; Chen, L. F.; Yang, H. J.; Li, Z.; Suchopar, A.; Richards, R. *Adv. Mater.* **2008**, 20 (2), 267−271.
(29) Patil, P. S.; Patil, P. R.; Kamble, S. S.; Pawar, S. H. *Sol. Energy Mater. Sol. Cells* **2000**, 60 (2), 143−153.
(30) Tebby, Z.; Babot, O.; Toupance, T.; Park, D. H.; Campet, G.; Delville, M. H. *Chem. Mater.* **2008**, 20 (23), 7260−7267.
(31) Tebby, Z.; Uddin, T.; Nicolas, Y.; Olivier, C.; Toupance, T.; Labrugere, C.; Hirsch, L. *ACS Appl. Mater. Interfaces* **2011**, 3 (5), 1485−1491.
(32) Sasi, B.; Gopchandran, K. G. *Nanotechnology* **2007**, 18 (11), 115613.

308

dx.doi.org/10.1021/am302097b | *ACS Appl. Mater. Interfaces* 2013, 5, 301−309

(33) Zhang, Z.; Shao, C.; Li, X.; Wang, C.; Zhang, M.; Liu, Y. *ACS Appl. Mater. Interfaces* **2010**, *2* (10), 2915−2923.

(34) Passerini, S.; Scrosati, B. *J. Electrochem. Soc.* **1994**, *141* (4), 889−895.

(35) Ho, S.-W.; Chu, C.-Y.; Chen, S.-G. *J. Catal.* **1998**, *178*, 34−38.

(36) Zhao, B.; Ke, X.-K.; Bao, J.-H.; Wang, C.-L.; Dong, L.; Chen, Y.-W.; Chen, H.-L. *J. Phys. Chem. C* **2009**, *113* (32), 14440−14447.

(37) Gonzalez-Elipe, A. R.; Holgado, J. P.; Alvarez, R.; Munuera, G. *J. Phys. Chem.* **1992**, *96*, 3080−3086.

(38) Uhlenbrock, S.; Scharfschwerdt, C.; Neumann, M.; Illing, G.; Freund, H.-J. *J. Phys.: Condens. Matter* **1992**, *4*, 7973−7978.

(39) Nandy, S.; Saha, B.; Mitra, M. K.; Chattopadhyay, K. K. *J. Mater. Sci.* **2007**, *42* (14), 5766−5772.

(40) Ai, L.; Fang, G. J.; Yuan, L. G.; Liu, N. S.; Wang, M. J.; Li, C.; Zhang, Q. L.; Li, J.; Zhao, X. Z. *Appl. Surf. Sci.* **2008**, *254* (8), 2401−2405.

(41) Dutta, T.; Gupta, P.; Gupta, A.; Narayan, J. *J. Appl. Phys.* **2010**, *108* (8), 083715.

(42) Vanelp, J.; Searle, B. G.; Sawatzky, G. A.; Sacchi, M. *Solid State Commun.* **1991**, *80* (1), 67−71.

(43) Lee, S. H.; Joo, S. K. *Sol. Energy Mater. Sol. Cells* **1995**, *39* (2−4), 155−166.

(44) Scott, I. D.; Jung, Y. S.; Cavanagh, A. S.; Yan, Y.; Dillon, A. C.; George, S. M.; Lee, S. H. *Nano Lett.* **2011**, *11* (2), 414−418.

(45) Lee, S. H.; Cheong, H. M.; Liu, P.; Tracy, C. E.; Pitts, J. R.; Deb, S. K. *Solid State Ionics* **2003**, *165* (1−4), 81−87.

(46) Lee, S. H.; Cheong, H. M.; Liu, P.; Tracya, C. E. *Electrochem. Solid-State Lett.* **2003**, *6* (6), A102−A105.

(47) Wu, W. T.; Liao, W. P.; Chen, L. Y.; Chen, J. S.; Wu, J. J. *Phys. Chem. Chem. Phys.* **2009**, *11* (42), 9751−9758.